# Effects of terbium sulfide addition on magnetic properties, microstructure and thermal stability of sintered Nd–Fe–B magnets*

Xiang-Bin Li(李向斌)[1], Shuo Liu(刘硕)[1], Xue-Jing Cao(曹学静)[1,2], Bei-Bei Zhou(周贝贝)[1], Ling Chen(陈岭)[2], A-Ru Yan(闫阿儒)[2], and Gao-Lin Yan(严高林)[1,†]

[1] School of Physics and Technology, Wuhan University, Wuhan 430072, China

[2] Zhejiang Province Key Laboratory of Magnetic Materials and Application Technology, Ningbo Institute of Materials Technology and Engineering, Chinese Academy of Sciences, Ningbo 315201, China

(Received 2 January 2016; revised manuscript received 14 March 2016; published online 1 June 2016)

To increase coercivity and thermal stability of sintered Nd–Fe–B magnets for high-temperature applications, a novel terbium sulfide powder is added into $(Pr_{0.25}Nd_{0.75})_{30.6}Cu_{0.15}Fe_{bal}B_1$ (wt.%) basic magnets. The effects of the addition of terbium sulfide on magnetic properties, microstructure, and thermal stability of sintered Nd–Fe–B magnets are investigated. The experimental results show that by adding 3 wt.% $Tb_2S_3$, the coercivity of the magnet is remarkably increased by about 54% without a considerable reduction in remanence and maximum energy product. By means of the electron probe microanalyzer (EPMA) technology, it is observed that Tb is mainly present in the outer region of 2:14:1 matrix grains and forms a well-developed Tb-shell phase, resulting in enhancement of $H_A$, which accounts for the coercivity enhancement. Moreover, compared with $Tb_2S_3$-free magnets, the reversible temperature coefficients of remanence ($\alpha$) and coercivity ($\beta$) and the irreversible flux loss of magnetic flow ($h_{irr}$) values of $Tb_2S_3$-added magnets are improved, indicating that the thermal stability of the magnets is also effectively improved.

**Keywords:** terbium sulfide, magnetic property, microstructure, thermal stability

**PACS:** 75.50.Ww, 75.50.Vv, 71.20.Eh **DOI:** 10.1088/1674-1056/25/7/077502

## 1. Introduction

Since the invention of Nd–Fe–B magnets in 1984, the application of sintered Nd–Fe–B magnets has rapidly spread to various environmentally friendly fields such as driving motors for hybrid/electric vehicles and generators for wind turbines due to their excellent room-temperature magnetic property and low cost.[1–3] Unfortunately, the driving motors or generators often operate at high temperature, and their properties degrade rapidly because of poor temperature stability of NdFeB-type magnets. In order to improve its poor thermal performance, increased room temperature coercivity is desired to retain higher coercivity when it is used at elevated temperature. Recently, the achievable maximum energy product ($(BH)_{max}$) has reached 474 kJ/m$^3$, which is nearly equal to the theoretical value (525.4 kJ/m$^3$) of $Nd_2Fe_{14}B$ single crystal.[4] However, the practical coercivity of sintered magnets is only ~1/3–1/5 of the anisotropy field of the hard magnetic $Nd_2Fe_{14}B$ phase ($H_A = 5572$ kA/m).[5] Therefore, there is still a great potential for improving the coercivity of sintered Nd–Fe–B magnets, and a lot of efforts have been made in recent years.

As is known, substitution of heavy rare earth (HRE) elements such as Dy and/or Tb for Nd is an effective way to increase the coercivity of sintered Nd–Fe–B magnets as the magnetocrystalline anisotropy field of $Dy_2Fe_{14}B$ or $Tb_2Fe_{14}B$ is much higher than that of $Nd_2Fe_{14}B$.[6] Dy/Tb can be introduced into the magnet through the so-called grain boundary diffusion process (GBDP). By using dipping,[7] sputter deposition,[8] eletrophoretic deposition[9,10] for coating a thin layer of Dy-rich and/or Tb-rich on the surface of the Nd–Fe–B magnet and heat diffusion treatment, the coercivity can be greatly enhanced. However, these techniques can only be used for preparation of thin ($\leq$ 3 mm) magnets as the diffusion depth for the thermal diffusion of Dy and/or Tb into the magnet is limited. Another feasible method to introduce Dy/Tb is the addition of small amounts of Dy/Tb in the basic Nd–Fe–B alloy prior to sintering, such as $Dy_2O_3$,[11] $DyH_x$,[12] $DyF_3$,[13] DyN,[14] $Dy_{32.5}Fe_{62}Cu_{5.5}$,[15] $Dy_{69}Ni_{31}$,[16] and Dy/Tb nanoparticles.[17,18] With this method the coercivity of sintered Nd–Fe–B magnets can be increased without significant decrease in remanence due to the antiferromagnetic coupling between Fe and Dy/Tb. Moreover, this method is not restricted by the size of the magnets, which is beneficial for use in mass production.

In previous works, many researchers paid close attention to the HRE oxides, nitrides, and fluoride addition to improve the magnetic properties of Nd–Fe–B magnets and the effects of introduced elements other than Dy/Tb (such as O, F, and N) on the microstructure have been extensively studied.[11,13,14] However, few works about HRE sulfide addition have been done. In this paper, a novel $Tb_2S_3$ as the additive has been successfully introduced into the basic Nd–Fe–B magnets and the

*Project supported by the Science Funds from the Ministry of Science and Technology, China (Grant Nos. 2014DFB50130 and 2011CB612304) and the National Natural Science Foundation of China (Grant Nos. 51172168 and 51072139).

†Corresponding author. E-mail: gaolinyan@whu.edu.cn

© 2016 Chinese Physical Society and IOP Publishing Ltd 

related variation of the microstructure regarding the distribution of Tb and S has been studied. The effects of $Tb_2S_3$ addition on the magnetic properties and thermal stability were discussed based on the magnetic measurements and microstructural characterizations.

## 2. Experiment

An alloy with a nominal composition of $(Pr_{0.25}Nd_{0.75})_{30.6}Cu_{0.15}Fe_{bal}B_1$ (wt.%) was prepared by strip casting technique. The alloy strips were primarily crushed into coarse powders by hydrogen decrepitation (HD) process and then further milled into powders with an average particle size of ~3.0 μm by jet milling in a nitrogen atmosphere. Commercial $Tb_2S_3$ fine powders of 1.8 μm in particle size were uniformly blended with $(Pr_{0.25}Nd_{0.75})_{30.6}Cu_{0.15}Fe_{bal}B_1$ powder through a three-dimensional mixer in an argon atmosphere for 300 minutes. The completely mixed powders were compacted and aligned under a magnetic field of 1800 kA/m followed by isostatic pressing at 200 MPa. The resulting green compacts were sintered at 1025 °C for 2 h in a vacuum, followed by gas quenching (as-sintered state). Finally, the as-sintered magnets were annealed at 900 °C and 500–540 °C for 2 h, respectively.

Particle size distribution of the powders was measured by a laser diffraction particle size analyzer. Room temperature and elevated temperature magnetic properties of the prepared sintered magnets were measured with a NIM-500C magnetic measuring device after fully magnetizing, respectively. The irreversible loss of the magnetic flow was examined with a Helmholtz coil. The microstructures and element distributions of the polished samples were analyzed by field emission scanning electron microscope (FESEM, Zeiss SIGMA) and electron probe microanalyzer (EPMA, JXA-8230) equipped with an energy dispersive x-ray spectrometer (EDS, Oxford INCA X-act system) in high vacuum mode.

## 3. Results and discussion

### 3.1. Magnetic properties

Figure 1 shows the magnetic properties of sintered magnets as a function of $Tb_2S_3$ addition content. Compared with the $Tb_2S_3$-free sample, the coercivity ($H_{cj}$) of the magnets remarkably increases by about 37.2% (from 12.71 kOe to 17.44 kOe), when the $Tb_2S_3$ content increases from 0 to 1 wt.%, while maintaining a similar remanence ($B_r$) and an analogous inclination of the demagnetization curves (as shown in Fig. 2). As the $Tb_2S_3$ content increases further to 3 wt.%, the coercivity exhibits only 6.1% increment per mass percent (from 17.44 kOe to 19.57 kOe), meaning that there is little benefit to improve the coercivity of the magnets by further addition. Moreover, it is noted that the squareness of demagnetization curves slightly decreases when the content of $Tb_2S_3$ is more than 1 wt.% (see Fig. 2). In the meantime, it can be seen that $B_r$ and maximum energy product ($(BH)_{max}$) drop slightly with the further increase in the amount of $Tb_2S_3$ due to the magnetic dilution effect. It was therefore concluded that by unit amount of $Tb_2S_3$ addition, the magnet exhibits remarkable improvement in its coercivity without considerably sacrificing its remanence and maximum energy product.

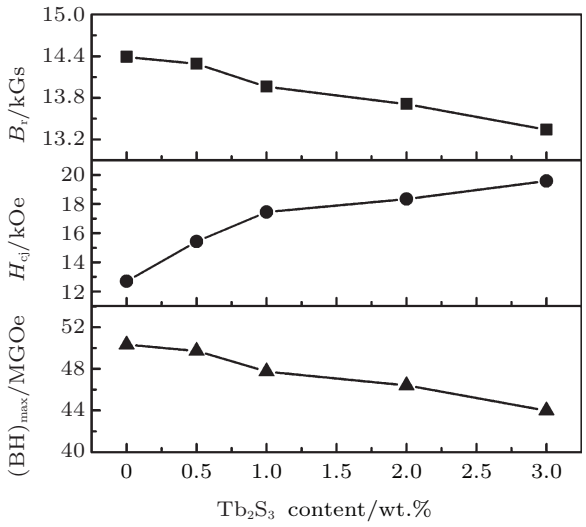



**Fig. 1.** The magnetic properties as a function of $Tb_2S_3$ content in the $(Pr_{0.25}Nd_{0.75})_{30.6}Cu_{0.15}Fe_{bal}B_1$ based sintered magnets.

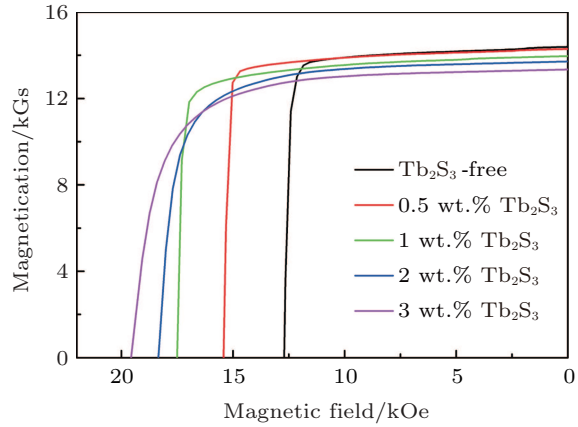



**Fig. 2.** (color online) Demagnetization curves of the basic $(Pr_{0.25}Nd_{0.75})_{30.6}Cu_{0.15}Fe_{bal}B_1$ magnet and the ones with different amounts of added $Tb_2S_3$.

### 3.2. Microstructure analysis

Figure 3 shows a typical back-scattered electron (BSE) SEM micrograph of Nd–Fe–B sintered magnet with 3 wt.% $Tb_2S_3$ addition. The bright contrast corresponds to the RE-rich phases. The dark gray contrast corresponds to the crystal grains of the 2:14:1 matrix phase. It was found that the bright RE-rich phase distributed homogeneously around the 2:14:1 matrix phase, resulting in a good decoupling between the neighboring matrix grains, which was favorable for coercivity of Nd–Fe–B magnet. In order to clarify the distribution of the introduced Tb and S elements in the Nd–Fe–B sintered

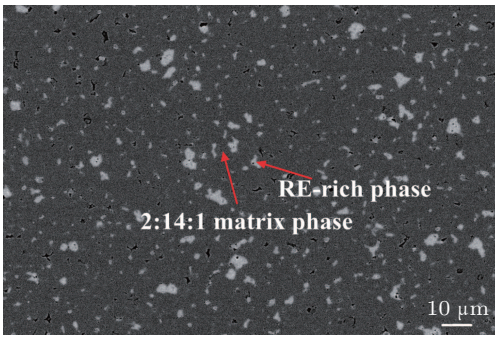



**Fig. 3.** (color online) Back-scattered electron (BSE) SEM micrograph of the 3 wt.% $Tb_2S_3$-added Nd–Fe–B sintered magnet.

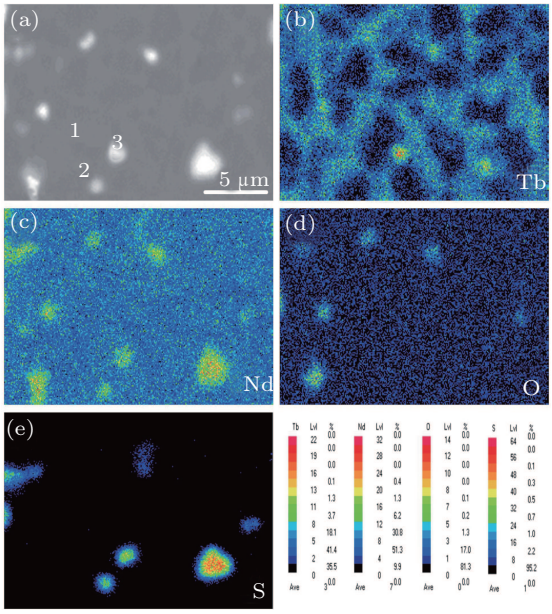



**Fig. 4.** (color online) (a) SEM image of the 3 wt.% $Tb_2S_3$-added magnet and concentration distribution mapping of (b) Tb, (c) Nd, (d) O, and (e) S elements in the Nd-rich phase and 2:14:1 matrix phase obtained from the same region as panel (a).

magnets, the concentration distribution of Tb, Nd, O, and S elements in the Nd-rich phase and 2:14:1 matrix phase was examined by electron probe microanalyzer (EPMA) and the results were shown in Fig. 4. It can be seen clearly that Nd, O, and S elements are mainly present at the triple junction of grain boundaries, and Tb element distributed mainly in the outer region of the 2:14:1 matrix grains, forming a so-called Tb-rich shell structure. Further quantitative investigation concentrations of Tb, Nd, O, and S in 2:14:1 matrix grain center and surface region, and in Nd-rich phase region, which were respectively marked by point 1, 2, 3 in Fig. 4(a), are summarized in Table 1. It is found that Tb concentration in the outer region of 2:14:1 grains (3.12 wt.%) is about eight times higher than those in the center of $Nd_2Fe_{14}B$ grains (0.40 wt.%), but much lower than those in the triple junction region (7.25 wt.%). The enriched Tb element in the outer region of 2:14:1 grains is expected to form a well-developed $(Nd,Tb)_2Fe_{14}B$ phase due to the substitution of Nd by Tb in $Nd_2Fe_{14}B$ compound. As is known, $(Nd,Tb)_2Fe_{14}B$ phase has a larger $H_A$ than that of the $Nd_2Fe_{14}B$ phase since the $H_A$ of 22.0 T for $Tb_2Fe_{14}B$ is much higher than that of 7.6 T for $Nd_2Fe_{14}B$.[6] As a consequence, $H_{cj}$ of the $Tb_2S_3$-added magnets is remarkably enhanced.

**Table 1.** Composition analyses results of the selected areas (1) 2:14:1 grain center, (2) 2:14:1 grain surface, and (3) Nd-rich triple junction phase for the magnet with 3 wt.% $Tb_2S_3$ addition.

| Position | Tb/wt% | Nd/wt% | Pr/wt% | O/wt% | Fe/wt% | S/wt% |
|---|---|---|---|---|---|---|
| 1 | 0.40 | 27.14 | 3.22 | — | 69.24 | — |
| 2 | 3.12 | 28.31 | 3.18 | — | 65.39 | — |
| 3 | 7.25 | 59.20 | 5.65 | 0.32 | 23.90 | 3.68 |

Moreover, S is only detected in the triple junction of grain boundaries, indicating that S in the $Tb_2S_3$ additives dissolves in the grain boundary phase rather than the 2:14:1 matrix phase during the sintering process. In the meantime, it is found that some of the S enriched in O-containing Nd-rich phases, but the rest are present in O-free Nd-rich phases. This shows that a new oxysulfide grain boundary phase may be $Nd_2O_2S$ emerging in O-containing Nd-rich phase, and an S-containing grain boundary phase may be NdS formed in O-free grain boundary phase. According to the report,[19] by introducing S element, HRE atoms would keep away from the oxysulfide and sulfide phases, which leads to more HRE diffusing into matrix grains, resulting in enhancement of $H_A$ (and as a consequence, $H_{cj}$).

### 3.3. Thermal stability

Table 2 shows the magnetic properties for the samples with different content of $Tb_2S_3$ addition at 20 °C and 100 °C, respectively. It can be seen that the magnetic properties of $Tb_2S_3$-free and $Tb_2S_3$-added magnets both decrease as the temperature increases to 100 °C. However, even at high temperatures (100 °C), $H_{cj}$ is significantly increased from 5.44 kOe to 10.86 kOe by adding 3 wt.% $Tb_2S_3$, meaning that the thermal stability of the magnet is effectively improved. In addition, based on these data, the reversible temperature coefficients of remanence ($\alpha$) and coercivity ($\beta$) of the magnets with different contents of $Tb_2S_3$ in the temperature range of 20–100 °C can be calculated with the equations[20] and the results as shown in Fig. 5. It was found that $\alpha$ values are improved from −0.116%/°C to −0.104%/°C in the range of 20–100 °C after adding 3 wt.% $Tb_2S_3$, and the corresponding $\beta$ values are improved from −0.763%/°C to −0.593%/°C. According to Refs. [11] and [21] the improvement of $\alpha$ can be attributed to the increased $T_c$ of matrix phase grains due to the partial substitution of Tb for Nd. At the same time, the improvement of $\beta$ is mainly attributed to the increased intrinsic property $H_A$ in this work. Therefore, decreased $\alpha$ and $\beta$ values further indicate that the thermal stability of sintered magnet can be significantly improved by $Tb_2S_3$ addition.

Furthermore, the irreversible loss of magnetic flow ($h_{irr}$) for the samples with different contents of $Tb_2S_3$ addition after exposure up to 150 °C for 2 h is shown in Fig. 6. It can be seen that $h_{irr}$ values for $Tb_2S_3$-free and $Tb_2S_3$-added magnets are

almost unchanged below 80 °C. When the exposure temperature increases to 150 °C, the $h_{irr}$ value of the $Tb_2S_3$-free magnet is about 34.57%. However, for the 3 wt.% $Tb_2S_3$-added magnet, $h_{irr}$ value is about 2.79% after exposure to 150 °C, which is much lower than that of the $Tb_2S_3$-free magnet. It is therefore concluded that the improvement of thermal stability of the magnet can be achieved through $Tb_2S_3$ addition.

**Table 2.** Magnetic properties of sintered samples as a function of $Tb_2S_3$ adding content at 20 °C and 100 °C, respectively.

| $Tb_2S_3$ content /wt.% | $B_r$/kGs | | $H_{cj}$/kOe | |
|---|---|---|---|---|
| | 20 °C | 100 °C | 20 °C | 100 °C |
| 0 | 14.39 | 13.14 | 12.71 | 5.44 |
| 0.5 | 14.29 | 13.05 | 15.43 | 7.90 |
| 1 | 13.96 | 12.84 | 17.44 | 9.20 |
| 2 | 13.71 | 12.63 | 18.35 | 9.73 |
| 3 | 13.34 | 12.30 | 19.57 | 10.86 |

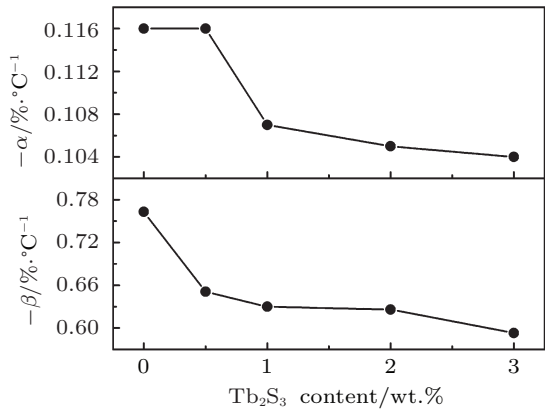



**Fig. 5.** Temperature coefficients of remanence ($\alpha$) and coercivity ($\beta$) of the magnets with different contents of $Tb_2S_3$ in the temperature range of 20–100 °C.

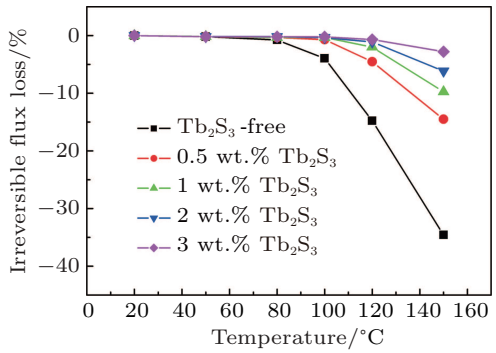



**Fig. 6.** (color online) The irreversible loss of magnetic flow for the samples with different contents of $Tb_2S_3$ addition after exposure up to 150 °C for 2 h.

## 4. Conclusion

The magnetic properties, microstructure, and thermal stability of the sintered magnets with terbium sulfide powder addition are systematically investigated, respectively. By adding 3 wt.% $Tb_2S_3$, the coercivity of the magnet is remarkably increased by about 54% without a considerable reduction in remanence and maximum energy product. The enhancement of coercivity can be attributed to the distribution of Tb and S element. Furthermore, the temperature-dependent magnetic properties indicate that the thermal stability of the Nd–Fe–B sintered magnet is effectively improved by $Tb_2S_3$ addition.

## Acknowledgment

We acknowledge the Ningbo Institute of Materials Technology and Engineering, Chinese Academy of Sciences for providing experimental facilities.

## References

[1] Sagawa M, Fujimura S, Togawa N, Yamamoto H and Matsuura Y 1984 *J. Appl. Phys.* **55** 2083
[2] Croat J J, Herbst J F, Lee R W and Pinkerton F E 1984 *J. Appl. Phys.* **55** 2078
[3] Wang X L, Zhao L N, Ding K H, Cui S L, Sun Y C and Li M S 2015 *Chin. Phys. B* **24** 037506
[4] Matsuura Y 2006 *J. Magn. Magn. Mater.* **303** 344
[5] Hono K and Sepehri-Amin H 2012 *Scr. Mater.* **67** 530
[6] Hirosawa S, Matsuura Y, Yamamoto H, Fujimura S, Sagawa M and Yamauchi H 1986 *J. Appl. Phys.* **59** 873
[7] Bae K H, Kim T H, Lee S R, Namkung S and Jang T S 2013 *IEEE Trans. Magn.* **49** 3251
[8] Li D, Suzuki S, Kawasaki T and Machida K 2008 *Jpn. J. Appl. Phys.* **47** 7876
[9] Soderžnik M, Rožman K Ž, Kobe S and McGuiness P 2012 *Intermetallics* **23** 158
[10] Cao X J, Chen L, Guo S, Li X B, Yi P P, Yan A R and Yan G L 2015 *J. Alloy. Compd.* **631** 315
[11] Cui X G, Cui C Y, Cheng X N and Xu X J 2014 *Intermetallics* **55** 118
[12] Yan G L, McGuiness P J, Farr J P G and Harris I R 2010 *J. Alloy. Compd.* **491** L20
[13] Xu F, Zhang L T, Dong X P, Liu Q Z and Komuro M 2011 *Scr. Mater.* **64** 1137
[14] Liu Q Z, Zhang L T, Xu F, Dong X P, Wu J S and Komuro M 2010 *Jpn. J. Appl. Phys.* **49** 093001
[15] Liang L P, Ma T Y, Zhang P, Jin J Y and Yan M 2014 *J. Magn. Magn. Mater.* **355** 131
[16] Liu X L, Wang X J, Liang L P, Zhang P, Jin J Y, Zhang Y J, Ma T Y and Yan M 2014 *J. Magn. Magn. Mater.* **370** 76
[17] Liu W Q, Sun H, Yi X F, Liu X C, Zhang D T, Yue M and Zhang J X 2010 *J. Alloy. Compd.* **501** 67
[18] Yue M, Liu W Q, Zhang D T, Jian Z G, Cao A L and Zhang J X 2009 *Appl. Phys. Lett.* **94** 092501
[19] Gabay A M, Marinescu M, Li W F, Liu J F and Hadjipanayis G C 2011 *J. Appl. Phys.* **109** 083916
[20] Brown D, Ma B M and Chen Z M 2002 *J. Magn. Magn. Mater.* **248** 432
[21] Gauder D R, Froning M H, White R J and Ray A E 1988 *J. Appl. Phys.* **63** 3522